Electron Energy-Loss Spectroscopy for Organic Compounds

Hiroki Kurata*, Seiji Isoda* and Takashi Kobayashi*

Electron energy-loss spectroscopy (EELS) combined with conventional transmission electron micros-copy has been applied to elemental microanalysis in thin films as well as investigations of local electro-nic structures. Recent development of parallel-EELS has opened up a road in the application of EELS to radiation sensitive materials like organic compounds. In this review paper, we describe firstly an orien-tation dependence of near-edge fine structures, which is generally expected for anisotropic materials like organic molecules. Secondly, the radiation damage process of phthalocyanine thin films studied through the change of near-edge fine structures obtained by EELS is presented. Finally, the elemental analysis of organic materials under restricted electron irradiation dosage because of their radiation damage is dis-cussed in relation to minimum detectable concentration.

KEY WORDS: Electron energy-loss spectroscopy / Radiation damage / Microanalysis / Near-edge fine structures / Detection limit

1. Introduction

Electron microscopy (EM) is an established technique to provide the structure prop-erties of thin specimens ; the high-resolution microscopy can be used to investigate the defect structures in many kinds of materials involving organic crystals with an atomic resolution.[1] On the other hand, in transmitted electrons through a thin specimen, there are not only elas-tically scattered electrons (Bragg diffractions in the case of crystals) but also inelastically scattered ones. The later ones have been treated as a deteriorating factor for an image qual-ity or a background noise in an electron microscopic image. However, the measurement of an energy loss caused by the inelastic scattering events in the specimen can provide useful in-formation about the chemical properties of materials. This is called the electron energy-loss spectroscopy (EELS) , which has been developed since the first measurement of spectrum from large specimen area by Ruthemann.[2]

Recently, by combining both the EM and EELS techniques, it has become possible to know the chemical properties from a sub-micron or nanometer specimen area. This method called the analytical electron microscopy (AEM)[3,4] has some advantages compared to other solid-state spectroscopies : (i) it provides a spectrum from a nanometer scale area of speci-men which can be characterized with imaging and diffraction modes of EM, and (ii) a wide energy range can be covered within one spectrum, which consists of valence and inner-shell electrons excitations. Because each element has characteristic inner-shell levels, one can easily perform quantitative chemical analysis on such a small area of specimen using an inner-shell electron excitation spectrum. Moreover, the electron energy-loss near-edge struc-

*倉田博基, 磯田正二, 小林隆史：Division of States and Structures II, Institute for Chemical Research, Kyoto University, Uji, Kyoto 611, Japan

tures (ELNES) observed in core-loss spectra have a wealth of information on the nature of chemical bonds as well as the local atomic arrangement around an atom excited by incident electrons.[5] This is basically identical with the x-ray absorption near-edge structures (XANES) observed with the synchrotron radiation beam.

In this review paper, we will describe characteristics of the inelastic scattering associated with inner-shell electron excitation, and then show applications of ELNES to anisotropic materials and to the study of electron radiation damage of organic compounds. Finally, we will discuss the quantitative elemental microanalysis and its detection limit especially for the case of organic specimen. The brief description of the AEM instrument used here is shown in the following section.

2. Instrumentation

Since the first attempt to incorporate an electron spectrometer in a transmission electron microscope by Marton,[6] many types of AEM have been developed. Figure 1 shows a typical
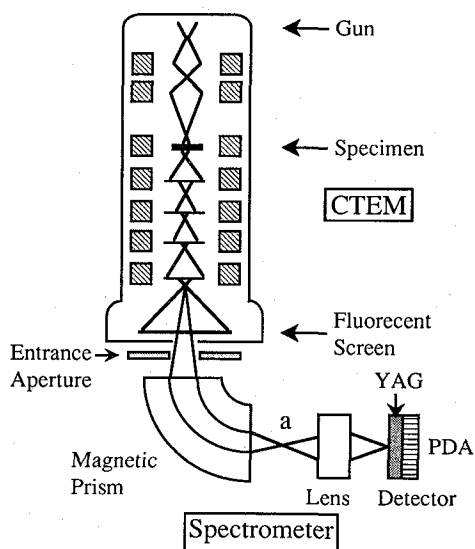

Figure 1 : Schematic representation of analytical electron microscope. Electron spectrometer consisting of a magnetic-prism, a lens system and a solid-state detector is mounted under a 200 kV conventional transmission electron microscope (CTEM).

modern AEM based on a conventional transmission electron microscope (CTEM). A simple magnetic-prism electron spectrometer is mounted beneath a CTEM column as a post-column analyzer, so that all of the functions of CTEM are held in this instrument ; images or diffraction patterns are observed on a fluorescent screen, which are used for the identification of a specimen area to be analyzed. If a fluorescent screen is taken off, electrons passing through an entrance aperture of spectrometer are energetically dispersed by the magnetic-prism and an EELS spectrum is imaged on an image point "a". This spectrum image is magnified by a lens system after the image point and then transformed into an optical signal by a YAG scintillator, which is finally counted using a 1024-elements linear photodiode array (PDA). Since such so-called parallel-recording system makes it possible to measure a spectrum within a very short time compared to previous serial-detection systems, it can be possible to study the radiation damage for electron sensitive materials by the parallel-EELS.

Spectra shown in the present paper were measured using a JEM-2000FXII equipped with a Gatan parallel-EELS device.[7] The energy resolution defined by the full width at half maximum of a zero-loss peak is mainly governed by the natural energy spread of a primary beam emitted from a LaB_6 filament, which is about 1eV. When the spectrum is measured with the diffraction mode at which a diffraction pattern is observed on a fluorescent screen, one can record an angle resolved spectrum, while a spatially resolved spectrum can be obtained with the image mode. In both cases, the spectrum can be measured from the same area that the image or diffraction pattern is observed, which is a prominent characteristic of this instrument.

3. Inelastic scattering cross-section for inner-shell electron excitation

In the framework of the first Born-approximation, the inelastic scattering cross-section concerning the transfers of energy E and momentum $\hbar q$ for high energy incident electron is expressed by the energy-loss function, $Im[-1/\varepsilon(q,E)]$,[4]

$$\frac{\partial^2 \sigma}{\partial E \partial \Omega} = \frac{1}{\pi^2 a_0^2 e^2} \cdot \frac{1}{q^2} \cdot Im\left[-\frac{1}{\varepsilon(q,E)}\right] \tag{1}$$

where a_0 is the Bohr radius and $\varepsilon(q,E)$ the complex dielectric response function of solid. The energy-loss function is given by

$$Im\left[-\frac{1}{\varepsilon(q,E)}\right] = \frac{\varepsilon_2}{\varepsilon_1^2 + \varepsilon_2^2} \tag{2}$$

where ε_1 and ε_2 are a real and an imaginary part of the complex dielectric function, respectively. In the case of high energy transfer which corresponds mainly to the inner-shell electron excitation, the value of ε_1 becomes almost unity, while the ε_2 value is much smaller than unity. Therefore, the energy-loss function is approximately equal to the imaginary part of the complex dielectric function, which reflects the optical absorption spectrum for solid. Within the approximation of one-electron transition between an initial state of ϕ_i and a final state ϕ_f of the electron in solid, the $\varepsilon_2(q,E)$ is given by

$$\varepsilon_2\left(q, E\right) = \frac{4\pi^2 e^2}{q^2} \cdot \sum_{i,f} \left| \langle \phi_f | \sum_j e^{iq\cdot r_j} | \phi_i \rangle \right|^2 \cdot \delta\left(E_f - E_i - E\right) \tag{3}$$

Practically, in the case of inner-shell electron excitation spectrum one refers the specific transition from an initial state with principal n and angular momentum l quantum numbers to a final state with n' and l' quantum numbers. Consequently, the inelastic scattering cross section for inner-shell electron excitation is represented by

$$\frac{\partial^2 \sigma}{\partial E \partial \Omega} = \frac{4}{a_0^2 q^4} \cdot \sum_{l'} \left| \langle n', l' | e^{iq\cdot r} | n, l \rangle \right|^2 \cdot \delta\left(E_{n', l'} - E_{n, l} - E\right) \tag{4}$$

In the small angle limit, the exponential term can be expanded as $e^{iq\cdot r} = 1 + iq\cdot r + \cdots$ and the matrix element can be approximated to

$$\left| \langle n', l' | e^{iq\cdot r} | n, l \rangle \right|^2 = q^2 \cdot \left| \langle n', l' | \mathbf{u}\cdot\mathbf{r} | n, l \rangle \right|^2 \tag{5}$$

where the vector u is a unit vector of momentum transfer $\hbar q$. This matrix element determines the selection rule for transition ; the dipole transition is only allowed, which means that the change of angular momentum quantum number should be $\Delta l = \pm 1$. Moreover, the density of states in equation (4)

$$\rho_{l'} = \delta\left(E_{n', l'} - E_{n, l} - E\right) \tag{6}$$

depends only on the angular momentum quantum number l' of the final state of transitions. Therefore, the fine structures observed on the near-edge region of each core-loss spectrum, ELNES, reflects the partial density of states of unoccupied bands allowed by the dipole selection rule. Because the wave function of initial core-state is spatially localized, the matrix element in equation (5) is mainly determined by terms from the near-neighboring atoms around an excited atom. This fact is the reason why the near-edge fine structures can be used as a so-called fingerprint to investigate the local symmetry and chemical bonding around an excited atom.[8]

Within the small angle scattering limit, the ELNES is basically identical with x-ray absorption near-edge structures. The momentum transfer $\hbar q$ in the EELS experiment corresponds to the polarization vector of synchrotron radiation beam on the x-ray absorption spectroscopy. In the case of K-edge spectra for anisotropic materials like a graphite, one can expect that the matrix element of equation (5) should be sensitive to the direction of the momentum transfer relative to a certain crystal orientation. Such an orientation dependence of ELNES is discussed in detail in the following section.

4. Orientation dependence of ELNES

Figure 2 shows the carbon K-edge spectra of graphite measured as a function of an orientation angle α between the crystal c-axis and the vector of momentum transfer. The scattering geometry in the present experiment is shown in the inset of Fig. 2. The measure-

ments for a different orientation angles were performed with the diffraction mode by taking a spectrum with a different scattering angle θ determined from a diffraction pattern, where an orientation angle α was estimated from the θ using the following relation

$$\alpha = \tan^{-1}\left(\frac{\theta}{\theta_E}\right) \tag{7}$$

Here θ_E is a characteristic angle defined by $E/2E_0$, where E and E_0 are a loss of energy and an energy of primary beam, respectively.

Both the fine structures and their intensity vary with the orientation angle. The ELNES features can be interpreted by density of states (DOS) of unoccupied bands. From a correspondence between the experimental spectrum and the DOS spectrum of unoccupied bands for graphite calculated by Willis et al.,[9] peaks A, C and H are attributed to the transitions from an initial 1s state to unoccupied π^*-bands, while the rest is assigned to 1s$\rightarrow \sigma^*$ transitions. The intensities of 1s$\rightarrow \pi^*$ transition peaks are rapidly decreased with the orientation angle, which is interpreted by an effect of the matrix element in the inelastic scattering cross-section. The wave function of the final state for 1s $\rightarrow \pi^*$ transition can be expressed
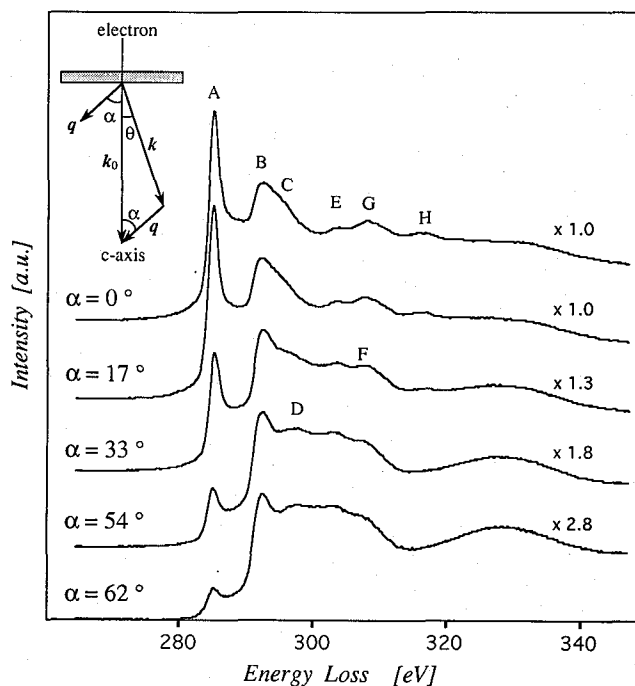
Figure 2 : Carbon K-edge ELNES of graphite as a function of an orientation angle α between momentum transfer and the crystal c-axis. Scattering geometry in the present experiment is shown in the inset.

as Bloch functions with the $2p_z$ atomic orbitals directing to the c-axis. Because the initial core-state is spatially localized, the main contribution to the matrix element comes from the

overlap between the initial 1s-state and the $2p_z$ atomic orbital localized on the excited atom. Therefore, within this on-site approximation, the inelastic scattering cross-section depends on an direction of the momentum transfer with respect to $2p_z$ orbital, i.e. the c-axis of graphite crystal. In the present scattering geometry as shown in the inset of Fig. 2, the angular dependence of equation (4) can be represented as $\cos^4 \alpha$. Fig. 3 shows the intensity of
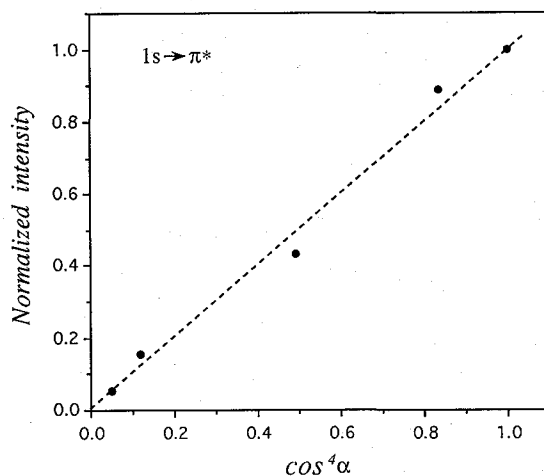

Figure 3 : Relative intensity of peak A $(1s \rightarrow \pi^*$ tran-sition) as a function of $\cos^4 \alpha$.

peak A $(1s \rightarrow \pi^*$ transition) normalized by that of $\alpha = 0°$ as a function of $\cos^4 \alpha$. The linearity shown in Fig. 3 indicates clearly the strong orientation dependence of peak A as discussed here, which suggests that the on-site approximation is appropriate to the analysis of ELNES.

   Such an orientation dependence of the $1s \rightarrow \pi^*$ transition peak is generally expected for molecules possessing a conjugated π-electron system. Because of the definite directionality of a final state concerned in the transition, this strong orientation dependence can be used to determine the structural properties, for example, the determination of molecular orientation on surfaces.[10] We have successfully applied it to determine the structure of potassium-benzene-graphite intercalation compound,[11] in which the molecular orientation of benzene intercalated between graphite layers has been decided by analyzing an orientation dependence of the $1s \rightarrow \pi^*$ transition peak quantitatively. This suggests that the ELNES spectroscopy is a powerful tool for investigation of structural properties as well as chemical bonding of materials.

5. Radiation damage of organic molecules

Organic compounds are generally very sensitive to an electron irradiation, which makes a measurement of EELS spectrum difficult. However, recent developments of the parallel-EELS enable us to collect ELNES data quickly for radiation-sensitive materials. In this section, we describe an application of ELNES to investigate a mechanism of radiation damage for phthalocyanine derivatives.[12]
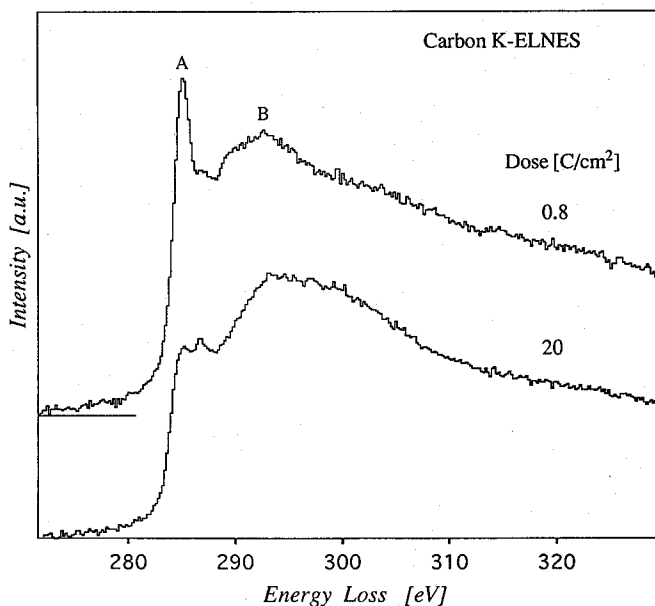
Figure 4 : Carbon K-edge spectrum of poly GeO-Pc measured after total dose of 0.8 and 20 C/cm². Peaks (A) and (B) are attributed to π^* and σ^* transitions, respectively by confirming an orientation dependence for each peak.

Fig. 4 represents typical spectra of carbon K-edge ELNES recorded from polymeric Ge-O-phthalocyanine (poly GeO-Pc) thin film with different electron irradiation doses. The ELNES features in an energy region up to about 20 eV above the carbon K-edge threshold are changed with an increase of irradiation dose, but no further change of this features was observed at doses higher than 20 C/cm². The first ELNES peak (A) and broad maximum (B) around 295 eV were attributed to the transition to π^* and σ^* unoccupied molecular orbitals respectively by analyzing the orientation dependence of these peaks in the same method as mentioned in the last section. Fig. 5 shows the difference spectra obtained by subtracting the final spectrum after 20 C/cm² dose from each spectrum at several stages during an electron irradiation. In this figure the intensity of the π^* peak (A) decreased gradually with an electron irradiation, while the σ^* peak (B) increased, which suggests that some of π bonds changed into σ bonds by an electron irradiation. It is also noticed that the integrated intensity in the energy-loss region extending to 60 eV from the threshold changes very little during an irradiation, which means that no loss of carbon atoms occurred in the
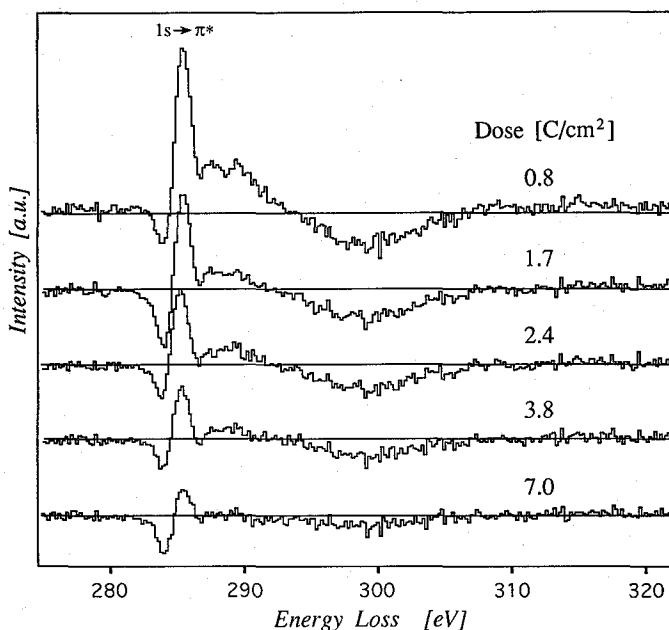
Figure 5 : Difference spectra obtained by subtracting the spectrum
observed after 20 C/cm² from that at several stages dur-
ing an electron irradiation.

irradiated specimen area because the integrated intensity of a core-loss spectrum is prop-
ortional to the number of atoms giving rise to the ionization peak.[4]

The nitrogen K-ELNES measured at the low dose of 0.8 C/cm² is shown in Fig. 6. Lit-
tle change of the ELNES feature was observed at further irradiation doses without a decrease
of integrated intensity. The intensity of the first ELNES peak is assigned to the π^*
transition, but it seems to decrease already even at the low dose of 0.8 C/cm². The fading of
this peak in the nitrogen K-ELNES is rapid compared to that in the carbon K-ELNES, which
suggests an existence of a site-dependent mechanism in the damage of molecular structure.

Moreover, we have performed the same experiments on a chlorinated copper- phthalocy-
anine (Cu-Pc) thin film which is known as the remarkable high resistant molecule to an elec-
tron irradiation among organic compounds. In this case it has been observed that the intensi-
ties of $1s \to \pi^*$ transition peak on carbon and nitrogen K-edges fade with the same rate and
more slowly than those in the poly GeO-Pc. Fig. 7 shows the dose-response curve on the
base of the fading of $1s \to \pi^*$ transition intensity of poly GeO-Pc and chlorinated Cu-Pc
molecules. From this figure it can be understood that the effect of substitution of the hyd-
rogen atoms by chlorine atoms is noticeable in radiation damage ; the chlorinated Cu-Pc is
more radiation resistant than the poly GeO-Pc by more than one order of magnitude.
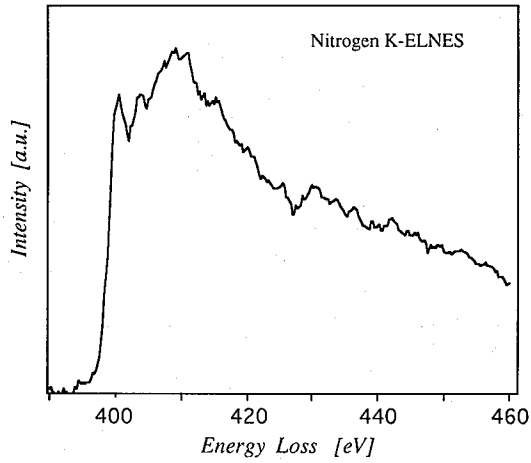
Figure 6 : Nitrogen K-edge spectrum of poly GeO-Pc me-
asured after total dose of 0.8 C/cm^2. Little
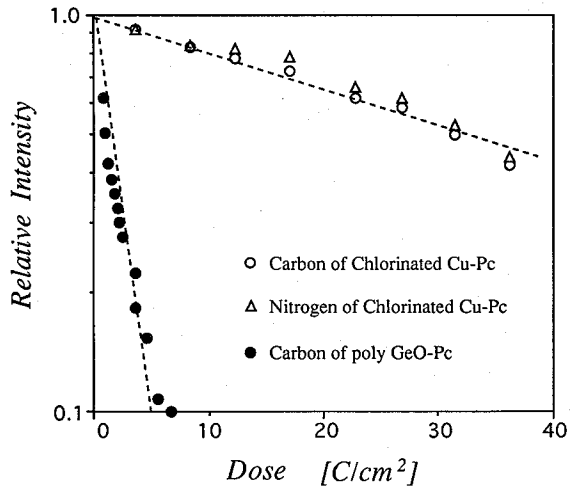change in the ELNES was observed at further
irradiation dose.

Figure 7 : Dose-response curves obtained by fading of
the $1s \rightarrow \pi^*$ transition peak in carbon and
nitrogen K-edge of poly GeO-Pc and chlorin-

ated Cu-Pc.

The mechanism of radiation damage has been postulated that the primary reaction involves the cleavage of some chemical bonds mainly at molecular periphery (C-H or C-Cl), which is followed by the production of radicals caused by the dissociation of atoms.[13] The chlorine atoms liberated by the cleavage of C-Cl bonds are less mobile than the liberated H atoms because the large size of the Cl atom compared to the H atom restricts the diffusion in the intermolecular spaces. The immobility of the Cl atoms is likely to cause the C-Cl bonds to reform, which is a reason why the chlorinated Cu-Pc is highly resistant to electron beam. Moreover, the secondary damage caused by the liberated H atoms may advance the rate of damage of the poly GeO-Pc compared to the chlorinated Cu-Pc. This secondary damage by the liberated H atoms is probably an important process to understand the site-dependent damage mechanism observed in poly GeO-Pc as mentioned above.

With the support of molecular orbital (MO) calculations,[14] the final state of the $1s \rightarrow \pi^*$ transition peak can be attributed to the lowest unoccupied $7e_g$ orbital possessing a π polarization which means that the orbital consists of p_z atomic orbitals of carbon and nitrogen atoms. Within the on-site approximation, the peak intensity is related to the population of MO on each atomic site contributing the final state. The population analysis of the MO has revealed that the carbon atoms located in a pyrrole ring and the bridge-site nitrogen atoms of the Pc molecule contribute mainly to $7e_g$ orbital, which means that the $1s \rightarrow \pi^*$ transition intensity is insensitive to the cleavage of peripheral bonds. In this sense, the fading of $1s \rightarrow \pi^*$ transition intensity seems to indicate the damage on the inner part of molecule. Therefore, the difference between the decay rates of the $1s \rightarrow \pi^*$ transition peak of the nitrogen and the carbon K-edges of the poly GeO-Pc film may be caused by the secondary damage process; it can be proposed that the liberated H atoms could preferentially attack the nitrogen atoms located on the bridge-site of neighboring molecules in the poly GeO-Pc film. On the other hand, in the case of chlorinated Cu-Pc, no such secondary damage process is expected, so that the $1s \rightarrow \pi^*$ transition peaks of carbon and nitrogen fade slowly at the same damage rate.

The localized property of inner-shell electron excitation makes it possible to detect the damage process depending on the atomic site in molecule. The method presented here prefers to investigate the damage process of molecular structure, while the method analyzing the decay of a diffraction intensity gives an information on the damage of crystal structure. Moreover, because the integrated intensity of each core-loss peak relates to the number of atoms in an area examined, the quantitative analysis of core-loss peaks can be used for the measurement of mass-loss during an electron irradiation as well as elemental analyses. In the final section, we describe the microanalysis by the EELS and discuss on the detection limit in this method.

6. Elemental analysis

The advantage of EELS as a tool for elemental analysis is the capability of recording an rather wide energy range in one spectrum from a small specimen area. Fig. 8 shows a typic-

al spectrum from a chloro-tetraphenylporphynate-iron ($C_{44}H_{28}N_4ClFe$) thin film (20 nm thickness) .[15] The spectrum was measured from a 2 μ m diameter area with an acquisition time of 5 sec and a total irradiation dose of 0.3 C/cm^2. Core-loss peaks corresponding to all elements forming the molecule except for hydrogen are observed in this spectrum in addition to a small amount of oxygen impurity.

In Fig. 8, each core-loss peak is superimposed on a monotonically decreasing background which should be subtracted for a quantitative elemental analysis. The subtraction procedure was performed by approximating the background to a power-low energy dependence, AE^{-r}, where the coefficients of A and r are determined in the pre-edge region. The background contribution was extrapolated to the higher energy region beyond the ionization threshold and then subtracted from the measured spectrum. The extracted core-loss peaks are integrated with an energy width Δ which was set 50 eV in the present analysis.

The partially integrated intensity, $I_i(\beta, \Delta)$, of the core-loss peak of element i is related to the number of atom N_i through the following relation[4]
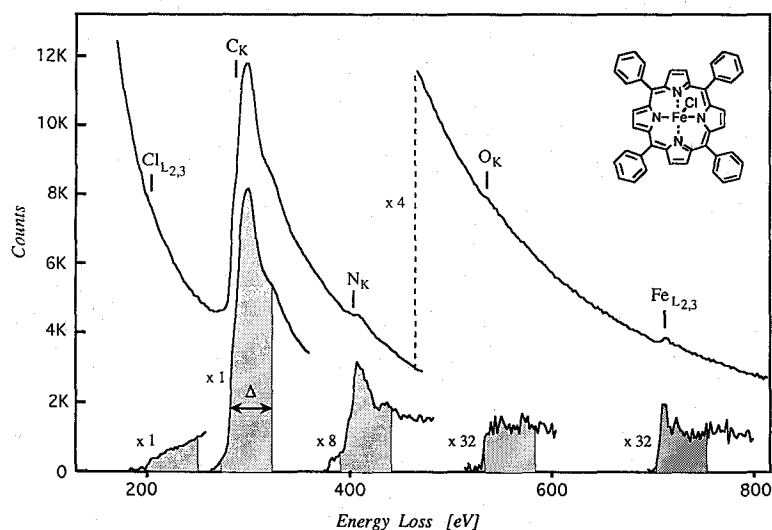

Figure 8 : Spectrum from chloro-tetraphenylporphynate-iron, showing Cl-$L_{2,3}$, C-K, N-K, O-K (due to a small amount of impurity) and Fe-$L_{2,3}$ edges. Quantitative analysis is performed for partially integrated intensities (hatched area with Δ = 50 eV window) after background subtraction.

$$I_i(\beta, \Delta) = D \cdot N_i \cdot \sigma_i(\beta, \Delta) \qquad (8)$$

where D is an electron dosage, $\sigma_i(\beta, \Delta)$ the partial inelastic cross-section and β collection angle (13 mrad in the present case) for recording a spectrum. The partial cross-section of each ionization edge is calculated using the SIGMAK and SIGMAL2 softwares written by Egerton.[4] From equation (8), the atomic concentration of element i, X_i, is deduced by

$$X_i = \frac{N_i}{N_t} = \frac{I_i(\beta,\Delta)/\sigma_i(\beta,\Delta)}{\sum_i\{I_i(\beta,\Delta)/\sigma_i(\beta,\Delta)\}} \qquad (9)$$

where N_t is the total number of atoms in an analyzed specimen area. The result of elemental analysis is summarized in Table 1, which agrees well with values expected from the molecular formula.

Table 1   Result of elemental analysis of chloro-tetraphenylporphynate-iron.Signal to noise ratio (SNR) of each core-edge was estimated using Egerton's Method.[16] Minimum detectable concentration,X_i^{min}, was determined from the X_i value for which SNR = (see text) .

	C	N	Cl	Fe	O
Observed $X_i$values [at%]	85.7	7.9	2.2	1.9	2.3
Calculated $X_i$values [at%]	88.0	8.0	2.0	2.0	—
SNR	1656	109	242	30	24
X_i^{min} [at%]	—	0.2	0.03	0.2	0.3

In order to estimate the minimum detectable concentration of element i, X_i^{min}, we follow the standard Egerton's statistical technique.[16] The signal to noise ratio (SNR) at a particular edge is given by

$$SNR = \frac{I_i}{(h \cdot I_b)^{1/2}} = \left(\frac{D \cdot N_t}{h \cdot \sigma_b}\right)^{1/2} \cdot X_i \cdot \sigma_i \qquad (10)$$

where I_b and σ_b are the background intensity and cross-section integrated on β and Δ, respectively, h is a factor representing statistical errors of background extrapolation. In the second equality the equation (8) is used for the intensities of signal and background. Using this relation the value of SNR at each edge was estimated from the experimental spectrum as shown in Table 1. The minimum detectable concentration can be calculated as the value of X_i^{min} for which SNR = 3 corresponding to 98% certainty for detection of the element, i.e.

$$X_i^{min} = \frac{N_i^{min}}{N_t} = \frac{3}{\sigma_i} \cdot \left(\frac{h \cdot \sigma_b}{D \cdot N_t}\right)^{1/2} \qquad (11)$$

The values of X_i^{min} estimated from this formula are also shown in Table 1. The elemental concentration of the order of 0.1 atomic % can be detectable under the present experimental conditions (D = 0.3 C/cm² and an analyzed area of 2 μm in diameter).

The X_i^{min} depends on an irradiation dosage and a diameter, d, of analyzed area through the total number of atoms ($N_t \propto d^2$). These two factors limit the minimum specimen area to be analyzed. The microanalysis for organic compounds is restricted by the largest permissible dose, which is the dosage not to induce a mass-loss of specimen under irradiation. Fig. 9 shows the minimum detectable concentration determined by measuring spectra as a function of a diameter d with a dose of 10 C/cm² of which any severe mass-loss does not detected in the present specimen, though the crystal structure is already destroyed. From this figure we can conclude that the microanalysis for a concentration of less than 1 atomic % can be performed on several tens nanometer of area with a dose of 10 C/cm². If more electrons is

permissible to irradiate on the specimen, the analyzed area could be reduced. For example, since iron atoms in this specimen little lose under a heavy electron irradiation, we confirmed experimentally that about 1 atomic % of iron in carbon matrix can be detected from an area of 5 nm in diameter with a dose of 200 C/cm^2, which corresponds to the detection of about 500 iron atoms.

The EELS combined with an electron microscope is a powerful tool not only for the quantitative microanalysis but also for the state analysis on a local area well-defined by TEM mode. Moreover, the image formation lens system incorporated in a EELS spectrometer will make it possible to produce an energy-selected image or an elemental mapping if a particular core-edge signal is used for imaging. Such a device is under development in our laboratory.
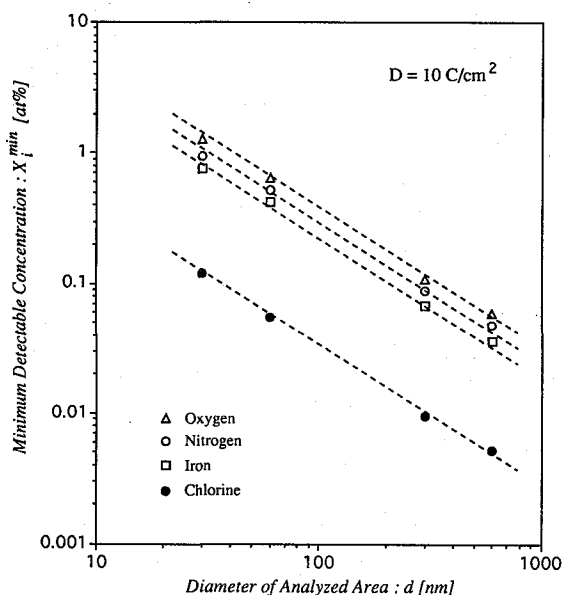

Figure 9 : Minimum detectable concentration, X_i^{min}, in a thin film of chloro- tetraphenylporphynate-iron as a func tion of diameter of analyzed area.

References

(1) T. Kobayashi and S. Isoda, *J. Mater. Chem.*, **3**, 1 (1993).
(2) G. Ruthemann, *Naturwissenschaften*, **30**, 145 (1942).
(3) C. Colliex, in: Advances in Optical and Electron Microscopy, Vol. 9, eds. R. Barer and V. E. Cosslett (Academic Press, London, 1984) p.65.
(4) R. F. Egerton, "Electron Energy-Loss Spectroscopy in the Electron Microscope" (Plenum Press, New York, 1986).
(5) H. Kurata, E. Lefèvre, C. Colleix, and R. Brydson, *Phys. Rev.,* **B 47,** 13763 (1993).
(6) L. Marton, *Rept. Prog. Phys.*, **10**, 205 (1946).
(7) O. L. Krivanek, C. C. Ahn and R. B. Keeney, *Ultramicroscopy*, **22**, 103 (1987).
(8) R. Brydson, H. Sauer, W. Engel, J. M. Thomas, and E. Zeitler, *J. Chem. Soc. Chem. Commun.,* **15**, 1010 (1989).

(9) R. F. Willis, B. Fitton, and G. S. Painter, *Phys. Rev.*, **B9**, 1926 (1974).

(10) J. Stöhr and D. A. Outka, *Phys. Rev.*, **B36**, 7891 (1987).

(11) H. Kurata, K. Ishizuka, T. Kobayashi, and N. Uyeda, *Synth. Met.*, **22**, 337 (1988).

(12) H. Kurata, S. Isoda, and T. Kobayashi, *Ultramicroscopy*, **41**, 33 (1992).

(13) J. R. Fryer, *Ultramicroscopy*, **14**, 227 (1984).

(14) F. W. Kutzler and D. E. Ellis, *J. Chem. Phys.*, **84**, 1033 (1986).

(15) H. Kurata, I. Kubo, S. Isoda, and T. Kobayashi, "Proc. 47-th Ann. Meet. Electron Micro. Soc. Jap," p.187 (1991).

(16) R. F. Egerton, *Ultramicroscopy*, **9**, 387 (1982).